Quantum phases of interacting bosons on biased two-leg ladders with magnetic flux

Xin Qiao, Xiao-Bo Zhang, Yue Jian, Ai-Xia Zhang, Zi-Fa Yu, and Ju-Kui Xue*
College of Physics and Electronics Engineering, Northwest Normal University, Lanzhou 730070, China

(Received 28 June 2021; revised 17 September 2021; accepted 10 November 2021; published 23 November 2021)

The realization and detection of various phase transitions in interacting two-leg bosonic flux ladders are at the frontier of the present theoretical and experimental research in condensed-matter physics. We develop a biased two-leg Bose-Hubbard flux ladder model and first achieve the ground states and phase transition conditions of this system by the mean-field approach and variational analysis. Rich phases are revealed, including two different kinds of plane-wave phase, i.e., plane wave I (characterized with one single energy minimum of the energy band) and plane wave II (characterized with two nondegenerate local energy minima of the energy band), and interestingly the asymmetry vortex phase with the breaking of both Z_2 reflection symmetry and translational symmetry of space, which is characterized by the vortex with imbalanced density distributions on two legs. Moreover, the corresponding quantum phases can also be distinguished by the order parameters and the excitation spectra of the plane-wave phase intuitively. Furthermore, we demonstrate that this biased ladder system also makes it possible to realize a different dynamical asymmetric vortex state, which shows a dynamical supersolidlike property.

DOI: 10.1103/PhysRevA.104.053323

I. INTRODUCTION

The most hallmark phenomenon of superconductors exposed to the external magnetic field $H < H_{c1}$ is the Meissner effect where the surface screening currents result a perfect diamagnet [1]. For type-II superconductors, a vortex phase exists when the field strength $H > H_{c1}$, in which magnetic flux partially penetrates the material [2]. The research of type-II superconductors looks very promising from the point of view of both fundamental science and applications. In ultracold atomic systems, the realization of artificial gauge fields [3–5] and optical lattices [6–8] provides an ideal platform with remarkable tunability to simulate such electronic phenomena of the strongly correlated system. Due to one-dimensional systems not having the orbital effect of the magnetic field, a two-leg ladder system [9–13] is the minimal setup for exploring complex phenomena of superconductivity. In addition, the ladder system also provides a fertile ground for studying common features of condensed-matter physics including some novel quantum phases [14–18], topological edge states [19–24], and many-body dynamics [25–29].

In recent years, the two-leg ladder system in the presence of an artificial gauge field has been successfully demonstrated in experiment [11,30–34]. In analogy to the type-II superconductor, the experiment [11] realized a quantum phase transition between the Meissner phase and vortex phase by manipulating the strength of the rung coupling, which also provided an efficient way to implement spin-orbit coupling (SOC) [35–37] in one-dimensional quantum gas. Combining the effects of the artificial gauge field and atomic interaction, tremendous activity in investigations is revealed using powerful theoretical and numerical methods in this system. Rich ground-state phase diagrams are the key task of this area, including superfluids, Mott insulators [14,38–41], vortex lattices [10,15,42,43], charge-density waves [44,45], and vortex density waves [46]. Furthermore, the possible existence of Laughlin-like states has drawn tremendous attention [47–53]. The ground-state properties under the finite-temperature [54] and the magnetic flux ramps [55] are also discussed in detail, respectively. Recently, an additional phase characterized by population imbalance between the two legs, named the biased ladder phase (BLP), has been predicted to be stable in the weakly interacting regime [56,57]. The BLP breaks global Z_2 reflection symmetry and enriches the ground state of the system.

In this paper, we propose a biased ladder system by detuning the Raman lasers to add a controlled energy bias between the two legs. The energy bias we introduced is analogous to the Zeeman field in SOC Bose-Einstein condensates (BECs). Currently, many theoretical and experimental research works have already confirmed that the Zeeman field plays a crucial role in SOC BECs, which leads to rich phase transition processes [35,36,58,59]. Accordingly, one can expect that this biased ladder system offers great potential for the appearance of novel phases and can be easily observed in current experiments. The ground states and the phase transition conditions of the biased ladder system are obtained analytically by the mean-field approach and variational analysis in this paper. We identify rich phases, including two different kinds of plane-wave phase, i.e., plane wave I (PWI, characterized with one single energy minimum of the energy band) and plane wave II (PWII, characterized with two nondegenerate local energy minima of the energy band), and interestingly a phase named the asymmetry vortex phase (AVP) characterized by the asymmetry vortex with imbalanced density distributions

*Corresponding author: xuejk@nwnu.edu.cn

on two legs. This phase breaks both Z_2 reflection symmetry and translational symmetry of space. The order parameters of the biased ladder system can be used to identify different quantum phases. We further study the excitation spectra of the plane-wave phase; the negative excitation demonstrates the existence of the AVP. Moreover, a different type of dynamical asymmetric vortex state (DAVS), resembling dynamical supersolidlike properties, is predicted in this biased ladder system. Because of these unique dynamical properties, the DAVS may have some potential applications in quantum transport and the time crystal. The AVP and DAVS obviously further enrich the phase transition properties and dynamics of the ladder system.

The paper is organized as follows. In Sec. II, we introduce the biased two-leg flux ladder model, and show the key aspects of the single-particle spectrum of the system. In Sec. III, we investigate the full phase diagrams and the ground-state properties of different phases by using variational analysis, and also discuss the excitation spectra of the system. The DAVS is discussed in Sec. IV. The summary and outlook of our paper are included in Sec.V.

II. MODEL

As realized in experiment [11], the lattice configuration creates a one-dimensional array of isolated ladders in the xy plane of the three-dimensional lattice and the atomic interaction can be easily tuned by using Feshbach resonance technology [60]. By changing the frequency of a pair of running-wave beams, a controlled energy bias between the two legs of the ladder can be introduced. We consider the biased bosonic two-leg ladder system with a flux ϕ per plaquette created by laser-assisted tunneling [61,62]. Due to the magnetic flux being translational invariant, the hopping matrix elements of the Hamiltonian along legs become complex by means of a unitary transformation. Physical properties are unchanged in different gauge choices [20,22,44,63,64]. Here the Hamiltonian as leg gauge is

$$\begin{aligned} H = & -J\sum_m \left(e^{i\frac{\phi}{2}}\hat{a}^\dagger_{m+1,L}\hat{a}_{m,L} + e^{-i\frac{\phi}{2}}\hat{a}^\dagger_{m+1,R}\hat{a}_{m,R} + \text{H.c.}\right) \\ & - K\sum_m (\hat{a}^\dagger_{m,R}\hat{a}_{m,L} + \text{H.c.}) \\ & - \frac{1}{2}\omega\sum_m (\hat{a}^\dagger_{m,L}\hat{a}_{m,L} - \hat{a}^\dagger_{m,R}\hat{a}_{m,R}) \\ & + \frac{U}{2}(\hat{a}^\dagger_{m,L}\hat{a}^\dagger_{m,L}\hat{a}_{m,L}\hat{a}_{m,L} + \hat{a}^\dagger_{m,R}\hat{a}^\dagger_{m,R}\hat{a}_{m,R}\hat{a}_{m,R}), \end{aligned} \tag{1}$$

where $\hat{a}^\dagger_{m,\sigma}$ and $\hat{a}_{m,\sigma}$ are the bosonic operators at the mth lattice site of the left or right leg (corresponding to $\sigma = L$ or R), ϕ is the magnetic flux per plaquette, ω is the controllable energy bias between the two legs, U is the strength of the atomic interaction, and K and J are tunneling amplitudes between nearest-neighbor sites across the rung and along the leg, respectively. Observables that can be readily measured in the experiment are the local currents on legs $j_\sigma(m) = iJ(e^{\pm i\frac{\phi}{2}}\hat{a}^\dagger_{m+1,\sigma}\hat{a}_{m,\sigma} - \text{H.c.})$ and rungs $j_{\text{rung}}(m) = iK(\hat{a}^\dagger_{m,R}\hat{a}_{m,L} - \text{H.c.})$ [11,23,43]. Apart from the configuration of local currents, the average current that circulates along the edge of the system $j_c = \frac{1}{N}\sum_m \langle j_L - j_R\rangle$, which is defined as the chiral current, also can be used to distinguish different phases in the two-leg ladder system. Using the mean-field approximation, we can neglect any thermal effect and obtain the mean-field approximation $\hat{a}_{m,\sigma} \simeq \langle \hat{a}_{m,\sigma}\rangle \equiv a_{m,\sigma}$. The discrete Gross-Pitaevskii (GP) equations associated with the Hamiltonian (1) can be written as

$$\begin{aligned} i\frac{\partial a_{m,L}}{\partial t} = & -J\left(e^{i\frac{\phi}{2}}a_{m-1,L} + e^{-i\frac{\phi}{2}}a_{m+1,L}\right) - Ka_{m,R} \\ & - \frac{1}{2}\omega a_{m,L} + U|a_{m,L}|^2 a_{m,L}, \\ i\frac{\partial a_{m,R}}{\partial t} = & -J\left(e^{-i\frac{\phi}{2}}a_{m-1,R} + e^{i\frac{\phi}{2}}a_{m+1,R}\right) - Ka_{m,L} \\ & + \frac{1}{2}\omega a_{m,R} + U|a_{m,R}|^2 a_{m,R}, \end{aligned} \tag{2}$$

where the unit is the natural unit $\hbar = 1$.

For noninteracting particles $\tilde{U} = 0$, we seek for plane-wave solutions $a_{m,\sigma} = a_\sigma e^{ikm}$, where k is the dimensionless quasimomentum, which is rescaled as $k \to kd/\pi$ (d is the lattice constant). The expression for energy eigenvalues $E_\pm$ reads

$$E_\pm = -2\cos k\cos\frac{\phi}{2} \pm \sqrt{\tilde{K}^2 + \frac{1}{4}\left(\tilde{\omega} + 4\sin k\sin\frac{\phi}{2}\right)^2}, \tag{3}$$

where the interaction-to-leg coupling ratio is $\tilde{U} = U/J$, the rung-to-leg coupling ratio is $\tilde{K} = K/J$, the bias-to-leg coupling ratio is $\tilde{\omega} = \omega/J$, and the energy is normalized by the unit of J. Figure 1 shows the energy band structure of the noninteracting ladder system. It is clear that there exists a critical value $\tilde{K}_c$ for the bifurcation of the band structure. With the increase of the $\tilde{K}$, the structure of the lower band changes from single-well to double-well structure. For the case $\tilde{\omega} = 0$ [see Fig. 1(a)], $k_{0-} = k_{0+} = \arccos\sqrt{\cos^2(\phi/2) + \tilde{K}/[4\tan^2(\phi/2)]}$, which means the energy band is symmetric with respect to $k = 0$. However, for the case $\tilde{\omega} \neq 0$ [see Fig. 1(b)], due to $k_{0-} \neq k_{0+}$ and $k_0 \neq 0$, the symmetry of the energy band is broken and there is an energy difference $\Delta E = E(-k_{0-}) - E(k_{0+})$ between the two minima of the lower band, which is induced by the existence of the energy bias.

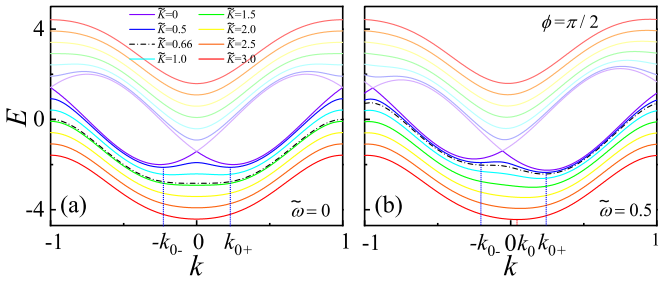

FIG. 1. Band structures of the noninteracting ladder system (a) $\tilde{\omega} = 0$ and (b) $\tilde{\omega} = 0.5$ for different rung-to-leg coupling ratios $\tilde{K}$.

III. PHASE DIAGRAM OF the BIASED LADDER SYSTEM

Affected by the atomic interaction together with the energy bias between the two legs, the low-energy band and the critical properties of the system will become more complex, thus some novel quantum phases will occur. To determine the ground states, we consider the wave function using a variational procedure based on the ansatz

$$\begin{bmatrix} a_{m,L} \\ a_{m,R} \end{bmatrix} = \begin{bmatrix} \sin\frac{\alpha_+}{2}\cos\theta e^{imk_+} + \cos\frac{\alpha_-}{2}\sin\theta e^{-imk_-} \\ \cos\frac{\alpha_+}{2}\cos\theta e^{imk_+} + \sin\frac{\alpha_-}{2}\sin\theta e^{-imk_-} \end{bmatrix}, \quad (4)$$

with the angle θ ($0 \leqslant \theta \leqslant \pi/2$), the quasimomentum $k_\pm$, and the coefficients $\sin\frac{\alpha_\pm}{2}$ as the variational parameters, which satisfy the normalization constraint. Note that, if the energy bias $\tilde{\omega} = 0$, one can find $\alpha_+ = \alpha_- = \alpha$ and $k_+ = k_- = k$, which is analogous to the variational approach of Refs. [65,66]. Therefore, we can expect that the composite effect of the energy bias and atomic interaction will induce novel quantum phase transition processes in this ladder system. Inserting the ansatz Eq. (4) into the Hamiltonian, the total energy can be written as

$$\begin{aligned} E = &-2\Big\{\cos^2\theta\Big[\sin^2\frac{\alpha_+}{2}\cos\Big(k_+ - \frac{\phi}{2}\Big) + \cos^2\frac{\alpha_+}{2}\cos\Big(k_+ + \frac{\phi}{2}\Big)\Big] \\ &+ \sin^2\theta\Big[\cos^2\frac{\alpha_-}{2}\cos\Big(k_- + \frac{\phi}{2}\Big) + \sin^2\frac{\alpha_-}{2}\cos\Big(k_- - \frac{\phi}{2}\Big)\Big]\Big\} \\ &- \tilde{K}(\sin\alpha_+\cos^2\theta + \sin\alpha_-\sin^2\theta) + \frac{\tilde{\omega}}{2}(\cos\alpha_+\cos^2\theta + \cos\alpha_-\sin^2\theta) \\ &+ \frac{\tilde{U}}{2}\Big[\Big(\sin^4\frac{\alpha_+}{2} + \cos^4\frac{\alpha_+}{2}\Big)\cos^4\theta + \Big(\sin^4\frac{\alpha_-}{2} + \cos^4\frac{\alpha_-}{2}\Big)\sin^4\theta \\ &+ \Big(\sin^2\frac{\alpha_+}{2}\cos^2\frac{\alpha_-}{2} + \cos^2\frac{\alpha_+}{2}\sin^2\frac{\alpha_-}{2}\Big)\sin^2 2\theta\Big]. \end{aligned} \quad (5)$$

By minimizing the total energy, the variational parameters $(k_\pm, \alpha_\pm, \theta)$ can be calculated, thus we can obtain key physical quantities of the biased ladder system. The density distributions are shown to be

$$\begin{aligned} n_{m,L} &= \sin^2\frac{\alpha_+}{2}\cos^2\theta + \cos^2\frac{\alpha_-}{2}\sin^2\theta + \sin\frac{\alpha_+}{2}\cos\frac{\alpha_-}{2}\sin 2\theta\cos\beta, \\ n_{m,R} &= \cos^2\frac{\alpha_+}{2}\cos^2\theta + \sin^2\frac{\alpha_-}{2}\sin^2\theta + \sin\frac{\alpha_+}{2}\cos\frac{\alpha_-}{2}\sin 2\theta\cos\beta, \end{aligned} \quad (6)$$

where $\beta = (k_+ + k_-)m$. Meanwhile, the local currents can be calculated as

$$\begin{aligned} j_{m,L} = &\ 2\sin^2\frac{\alpha_+}{2}\cos^2\theta\sin\Big(k_+ - \frac{\phi}{2}\Big) - 2\cos^2\frac{\alpha_-}{2}\sin^2\theta\sin\Big(k_- + \frac{\phi}{2}\Big) \\ &+ \sin\frac{\alpha_+}{2}\cos\frac{\alpha_-}{2}\sin 2\theta\Big[\sin\Big(k_+ - \frac{\phi}{2} - \beta\Big) - \sin\Big(k_- + \frac{\phi}{2} - \beta\Big), \\ j_{m,R} = &\ 2\cos^2\frac{\alpha_+}{2}\cos^2\theta\sin\Big(k_+ + \frac{\phi}{2}\Big) - 2\sin^2\frac{\alpha_-}{2}\sin^2\theta\sin\Big(k_- - \frac{\phi}{2}\Big) \\ &+ \sin\frac{\alpha_+}{2}\cos\frac{\alpha_-}{2}\sin 2\theta\Big[\sin\Big(k_+ + \frac{\phi}{2} - \beta\Big) - \sin\Big(k_- - \frac{\phi}{2} - \beta\Big), \\ j_{m,\mathrm{rung}} = &\ \tilde{K}\sin 2\theta\Big(\sin\frac{\alpha_+}{2}\sin\frac{\alpha_-}{2} - \cos\frac{\alpha_+}{2}\cos\frac{\alpha_-}{2}\Big)\sin\beta. \end{aligned} \quad (7)$$

The energy minimization with respect to $k_\pm$ yields the general relationship $k_\pm = -\arctan[\cos\alpha_\pm\tan(\phi/2)]$. By using this relationship and minimizing the total energy with respect to θ and $\alpha_\pm$, i.e., $\partial E/\partial\theta = 0$ and $\partial E/\partial\alpha_\pm = 0$, we can obtain

$$\sin 2\theta[(A_+ + A_-) + 2\tilde{U}\cos 2\theta(\sin^2\alpha_+ - 4\cos\alpha_+\cos\alpha_- + \sin^2\alpha_-)] = 0, \quad (8)$$

$$\tilde{\omega}\sin\alpha_+ + \cos\alpha_+\Big[2\tilde{K} + \sin\alpha_+\Big(\tilde{U}\cos^2\theta - \frac{4\sin\frac{\phi}{2}\tan\frac{\phi}{2}}{\sqrt{1+\cos^2\alpha_+\tan^2\frac{\phi}{2}}}\Big)\Big] - 2\tilde{U}\sin^2\theta\sin\alpha_+\cos\alpha_- = 0, \quad (9)$$

$$\tilde{\omega}\sin\alpha_- - \cos\alpha_-\Big[2\tilde{K} + \sin\alpha_-\Big(\tilde{U}\sin^2\theta - \frac{4\sin\frac{\phi}{2}\tan\frac{\phi}{2}}{\sqrt{1+\cos^2\alpha_+\tan^2\frac{\phi}{2}}}\Big)\Big] + 2\tilde{U}\cos^2\theta\sin\alpha_-\cos\alpha_+ = 0, \quad (10)$$

where $A_\pm = \pm 16 \cos\frac{\phi}{2}\sqrt{1+\cos^2\alpha_\pm \tan^2\frac{\phi}{2}} - 4\tilde{\omega}\cos\alpha_\pm \mp \tilde{U}\cos 2\alpha_\pm \pm 8\tilde{K}\sin\alpha_\pm$. From Eqs. (8)– (10), the variational parameters can be calculated, and one can obtain the ground-state features of the biased ladder system.

A. Plane-wave phase

For $\theta = 0$ (or $\pi/2$), the ground state of the system is the plane-wave phase, which takes place in a single plane-wave state with a nonzero quasimomentum. According to different features of the variational energy landscape, this phase can be distinguished as PWI and PWII. There exists a critical value $\tilde{K}_c^{\text{I-II}}$, which can be calculated from the energy minimization with respect to $\alpha_\pm$. In this case, Eqs. (9) and (10) can be simplified as

$$\tilde{\omega}\sin\alpha_\pm \pm \cos\alpha_\pm\left[2\tilde{K} + \sin\alpha_\pm\left(\tilde{U} - \frac{4\sin\frac{\phi}{2}\tan\frac{\phi}{2}}{\sqrt{1+\cos^2\alpha_\pm\tan^2\frac{\phi}{2}}}\right)\right] = 0, \tag{11}$$

where the sign of α is defined on the energy bias to leg coupling ratio $\tilde{\omega} > 0$ ($\theta = 0$) or $\tilde{\omega} < 0$ ($\theta = \pi/2$).

When $\tilde{K} > \tilde{K}_c^{\text{I-II}}$, the solution $\alpha_\pm$ for Eq. (11) only has one single value at the corresponding $k_\pm \neq 0$, which means that the energy band only has one single minimum and the ground state of the biased ladder system is in the PWI. The broken Z_2 reflection symmetry brings a density imbalance $\Delta n = \sum_m (n_{m,R} - n_{m,L})/N$ between the two legs, which serves as the order parameter for this phase [44]. From Eqs. (6) and (7), we can obtain that the particles are more populated on the right (left) leg for $\tilde{\omega} > 0$ ($\tilde{\omega} < 0$) and the density on either leg is uniform. Meanwhile, local currents have the same strength but opposite direction on two legs and the currents vanish on the rungs [see Fig. 2(a)]. In the limit $\tilde{\omega} = 0$, the single minimum $k_\pm = 0$ and the ground state enters the Meissner phase, where the density is evenly distributed on the ladder and currents on legs reach a maximum value [see Fig. 2(b)].

When $\tilde{K}_c^{\text{I-II}} > \tilde{K} > \tilde{K}_c^{\text{II-III}}$, the system will turn to the PWII. The solution $\alpha_\pm$ for Eq. (11) will correspond to two energy minima at k_+ and $-k_-$, respectively. As shown in Fig. 1(b), there exists an energy bias between the two momentum states, so the ground state of the ladder system will choose the one with lower energy. The distributions of the density and local currents are similar to the PWI, but the density imbalance between two legs is larger and the strength of the currents is smaller [see Fig. 2(c)]. For the case $\tilde{\omega} = 0$, two momentum states have twofold degeneracy and the ground state obeys the BLP [56], which has similar density and current structures with the plane-wave phase, but the density imbalance is the result of spontaneous breaking of Z_2 reflection symmetry [see Fig. 2(d)]. At this point, the critical condition between the Meissner phase and BLP can be analytically given as $\tilde{K}_c^{\text{I-II}} = -\frac{\tilde{U}}{2} + 2\sin\frac{\phi}{2}\tan\frac{\phi}{2}$.

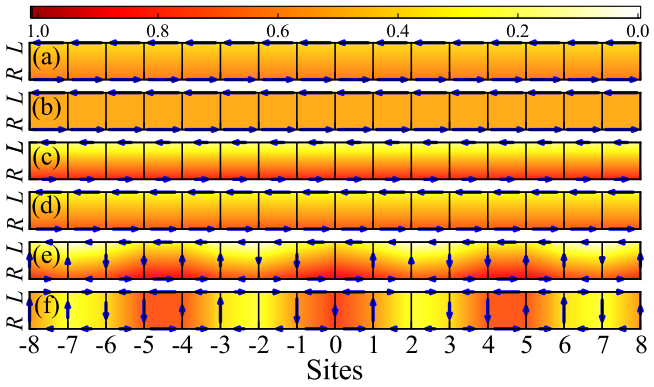

FIG. 2. Individual particle densities and currents for different phases. For the biased ladder $\tilde{\omega} = 0.2$, there are two kinds of plane-wave phase (a) PWI with $\tilde{K} = 1.5$, (c) PWII with $\tilde{K} = 0.75$, and a superposition state (e) AVP with $\tilde{K} = 0.65$. For the unbiased ladder $\tilde{\omega} = 0$, we show the (b) Meissner phase with $\tilde{K} = 1.5$, (d) BLP with $\tilde{K} = 1$, and (f) vortex phase with $\tilde{K} = 0.65$. The colorbar represents the particle density, blue arrows denote local currents, and the length of the arrow indicates the current strength, which is normalized to the local current of the Meissner phase. The other parameters are $\tilde{U} = 0.4$ and $\phi = \pi/2$.

B. Asymmetric vortex phase

When the strength of the atomic interaction increases further, the superposition state $\cos\theta|k_+\rangle + \sin\theta|-k_-\rangle$ of the ladder system will be the lowest-energy state, where $\tilde{K} < \tilde{K}_c^{\text{II-III}}$. From Eq. (8), we can obtain

$$\theta = \frac{1}{2}\arccos\left[\frac{A_+ + A_-}{2\tilde{U}(\sin^2\alpha_+ - 4\cos\alpha_+\cos\alpha_- + \sin^2\alpha_-)}\right], \tag{12}$$

which means this new ground state of the biased ladder system is the superposition state with different superposition coefficients. Meanwhile, the energy minimization with respect to $\alpha_\pm$ also gives Eqs. (9) and (10). By solving this set of equations, we can obtain the ground-state wave function. Particularly, the energy bias $\tilde{\omega}$ induces an asymmetric density modulation of the ladder system, which brings a different phase named the AVP. As shown in Fig. 2(e), the particle density distribution presents a spatial modulation on each leg and local currents exhibit a vortex structure in the ground state. The breaking of Z_2 symmetry leads to a density imbalance between two legs, and the current strength on two legs becomes different. When $\tilde{\omega} > 0$ ($\tilde{\omega} < 0$), the density and current strength on the right (left) leg are large. For the unbiased system, $k_+ = k_-$ and the angle $\theta = \pi/4$. Hence, the vortex structure at this point becomes symmetric, which accords with the ordinary vortex phase [see Fig. 2(f)]. This is a particular case of AVP without energy bias. In addition to the continuous $U(1)$ symmetry in the Meissner phase, these two kinds of vortex phase have a second spontaneous broken translational symmetry of space. Similar to the long-range spatial periodicity of solids, this density modulation combined with superfluid properties results in the supersolidity of the vortex phase [35,67].

By means of the variational approach, the full phase diagram in the presence of energy bias is summarized in Fig. 3.

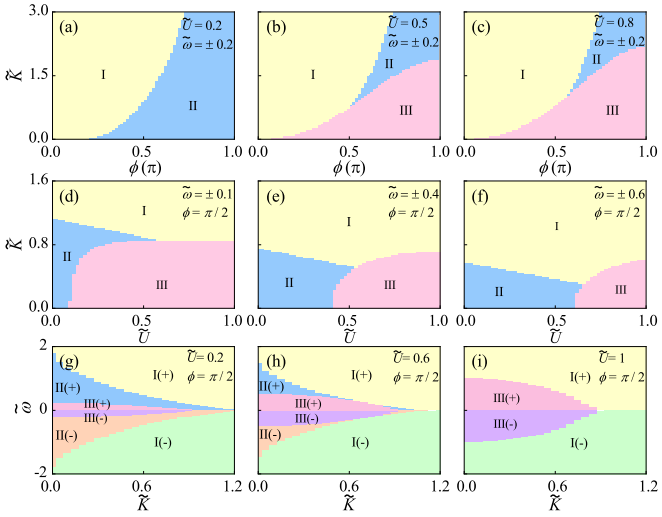

FIG. 3. Phase diagrams in the $\tilde{K}$-ϕ plane with different atomic interactions (a) $\tilde{U} = 0.2$, (b) $\tilde{U} = 0.5$, and (c) $\tilde{U} = 0.8$; phase diagrams in the $\tilde{K}$-$\tilde{U}$ plane with different energy biases (d) $\tilde{\omega} = \pm 0.1$, (e) $\tilde{\omega} = \pm 0.4$, and (f) $\tilde{\omega} = \pm 0.6$; and phase diagrams in the $\tilde{\omega}$-$\tilde{K}$ plane with different atomic interactions (g) $\tilde{U} = 0.2$, (h) $\tilde{U} = 0.6$, and (i) $\tilde{U} = 1$. The region I(±) and region II(±) correspond to two kinds of plane-wave phase PWI and PWII, respectively. The region III(±) corresponds to the AVP.

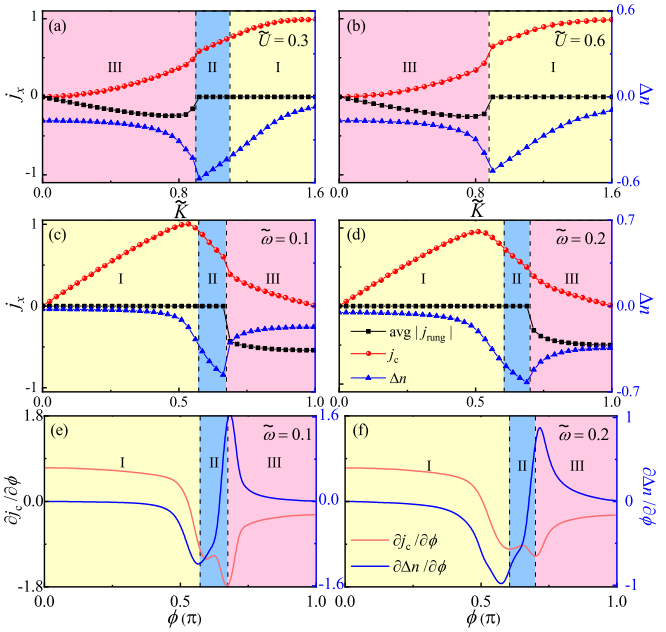

FIG. 4. Chiral current j_c (red solid circle line), average rung current avg$|j_{\text{rung}}|$ (black solid square line), and density imbalance Δn (blue solid triangle line) for different quantum phases; cut through the phase diagram of the $\tilde{K}$-$\tilde{U}$ plane ($\phi = \pi/2$) at $\tilde{\omega} = 0.1$ with (a) $\tilde{U} = 0.3$ and (b) $\tilde{U} = 0.6$ [see Fig. 3(d)], respectively; cut through the phase diagram of the $\tilde{K}$-ϕ plane ($\tilde{U} = 0.8$) at $\tilde{K} = 1.5$ with (c) $\tilde{\omega} = 0.1$ and (d) $\tilde{\omega} = 0.2$ [see Fig. 3(c)], respectively; and slopes of the chiral current $\partial j_c/\partial\phi$ (red line) and density imbalance $\partial\Delta n/\partial\phi$ (blue line) vs ϕ with (e) $\tilde{\omega} = 0.1$ and (f) $\tilde{\omega} = 0.2$, respectively.

As shown in Fig. 3(a), when the atomic interaction is small, the ground state of the ladder system is the plane-wave phase. According to features of the variational energy landscape, the biased ladder system will transform from PWI (yellow region I) to PWII (blue region II) with the increase of the intensity of the magnetic field. As the strength of the atomic interaction exceeds a critical value, the AVP (pink region III) appears at the area with the small coupling ratio $\tilde{K}$ and strong magnetic field ϕ [see Figs. 3(b) and 3(c)]. As shown in Figs. 3(d)–3(f), when the atomic interaction is small, the phase transition is from the AVP to PWII. With the increase of the atomic interaction, the direct phase transition from the AVP to PWI emerges in the biased ladder system. Comparing Figs. 3(d)–3(f), we can obtain that the increase of the energy bias between two legs of the ladder system will significantly suppress the appearance of the AVP. The full phase diagrams in the $\tilde{K}$-$\tilde{\omega}$ plane are shown in Figs. 3(g)–3(i) with different atomic interactions. When we choose a small energy bias, the phase transition from the plane-wave phase to the AVP occurs with decreasing coupling ratio $\tilde{K}$. The light green, orange, and purple areas are the negative range of these phases with the opposite quasimomentum. Moreover, with the increase of the atomic interaction, the area of the AVP increases, but the area of PWII decreases greatly and even disappears.

The phase transition of the biased ladder system also can be identified by the order parameters, which can be observed directly in experiments. As shown in Fig. 4(a), indicators of the AVP to plane-wave phase transition can be detected with a marked jump of the chiral current j_c, average rung current avg$|j_{\text{rung}}|$, and particle density imbalance Δn, which indicate a first-order phase transition. When the atomic interaction increases, the direct phase transition from the AVP to PWI emerges [see Fig. 4(b)]. Moreover, these order parameters also can be used to distinguish PWI and PWII, which have different features in the energy diagram. With the increasing coupling ratio $\tilde{K}$, the order parameters are continuous across the PWII to PWI boundary, which can be identified by the spinodal of j_c and Δn. Figures 4(c) and 4(d) focus on a horizontal cut through the phase diagram of the $\tilde{K}$-ϕ plane at $\tilde{K} = 1.5$. The order parameters are also continuous at the boundary between PWI and PWII and discontinuous at the boundary between the plane-wave phase and AVP. Note that the jumps decrease when the energy bias $\tilde{\omega}$ is increasing. In order to show the spinodal between PWI and PWII more clearly, we plot slopes of the chiral current $\partial j_c/\partial\phi$ and density imbalance $\partial\Delta n/\partial\phi$ in Figs. 4(e) and 4(f). The first extreme value points in its slopes indicate the location of the spinodal between PWI and PWII. Meanwhile, the phase transition points between the plane-wave phase and AVP can also be marked by the second extreme value points in these slopes. As shown in Figs. 4(e) and 4(f), these results are according with Figs. 4(c) and 4(d).

To demonstrate the existence of the AVP, we study the stability of Eq. (4) as $\theta = \pi/2(0)$; the perturbed ground state can be written as

$$\begin{bmatrix} a_{m,L}(t) \\ a_{m,R}(t) \end{bmatrix} = \begin{bmatrix} \cos\frac{\alpha_-}{2} + \delta a_{m,L}(t) \\ \sin\frac{\alpha_-}{2} + \delta a_{m,R}(t) \end{bmatrix} e^{i(km-\varepsilon t)}. \quad (13)$$

The perturbation terms are given by

$$\delta a_{m,\sigma}(t) = W_{q,\sigma} e^{i(qm-\delta\omega t)} + V^*_{q,\sigma} e^{-i(qm-\delta\omega t)}, \quad (14)$$

where W and V are the perturbation amplitudes, and q is the quasimomentum of the quasiparticle excitation, which is rescaled as $q \to qd/\pi$. The frequencies of the perturbation $\delta\omega$ and time t are normalized by the unit of J. Inserting this perturbed ground state into the GP equation (2) and retaining only terms linear in the perturbations, we can obtain the Bogoliubov–de Gennes (BdG) equations $\mathcal{H}\mathbf{\Psi} = \delta\omega\mathbf{\Psi}$, where $\mathbf{\Psi} = (W_L, W_R, V_L, V_R)^T$, with the BdG Hamiltonian

$$\mathcal{H} = \begin{pmatrix} H_L(k,q) & -\tilde{K} & \tilde{U}\cos^2\frac{\alpha_-}{2} & 0 \\ -\tilde{K} & H_R(k,q) & 0 & \tilde{U}\sin^2\frac{\alpha_-}{2} \\ -\tilde{U}\cos^2\frac{\alpha_-}{2} & 0 & -H_L(k,-q) & \tilde{K} \\ 0 & -\tilde{U}\sin^2\frac{\alpha_-}{2} & \tilde{K} & -H_R(k,-q) \end{pmatrix}, \tag{15}$$

where

$$H_L(k,q) = -\varepsilon - 2\cos\left(k+q-\frac{\phi}{2}\right) - \frac{\tilde{\omega}}{2} + 2\tilde{U}\cos^2\frac{\alpha_-}{2},$$
$$H_R(k,q) = -\varepsilon - 2\cos\left(k+q+\frac{\phi}{2}\right) + \frac{\tilde{\omega}}{2} + 2\tilde{U}\sin^2\frac{\alpha_-}{2}. \tag{16}$$

By diagonalizing the BdG equation, we obtain the spectrum of elementary excitations, which has been experimentally observed via the Bragg spectroscopy measurement in SOC Bose gases [68–70]. As shown in Figs. 5(a) and 5(c), the spectrum of the plane-wave phase shows a phonon-maxon-roton-like feature. When the rung-to-leg coupling ratio $\tilde{K}$ and the energy bias $\tilde{\omega}$ decrease, the excitation energy of the rotonlike minimum decreases. However, the further decrease of $\tilde{K}$ and $\tilde{\omega}$ leads to a negative energy, which indicates that the plane waves suffer an energetic instability. Similar to the spin-$\frac{1}{2}$ and spin-1 SOC systems, the instability implies the tendency to develop crystalline order in the system [68,69,71]. In this case, the superposition state is energetically preferred, thus we can obtain the phase boundary between the plane-wave phase and the AVP by the excitation spectrum as illustrated in Figs. 5(b) and 5(d). When the excitation spectrum has a negative energy, the ground phase transitions into the AVP, where the cross node corresponds to phase transition points in Figs. 5(a) and 5(c), respectively. Comparing to phase diagrams in Fig. 3, we can confirm that our analytical results agree well with the results of the phase boundary of the AVP determined by the energetic instability [see Figs. 5(b) and 5(d)].

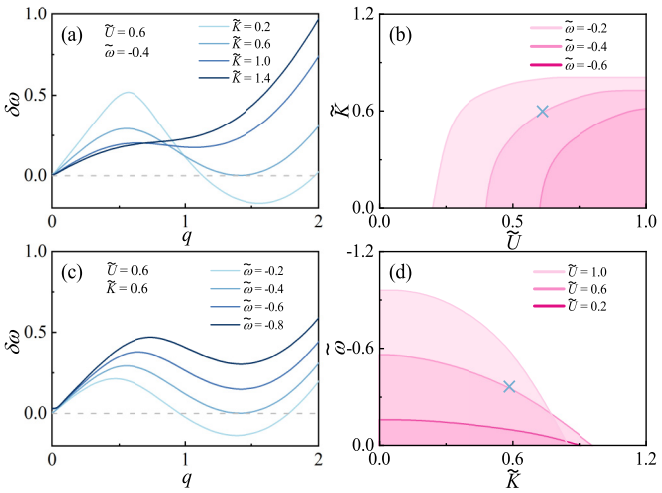

FIG. 5. Rotonlike minimum softening and energetic instability for decreasing (a) rung-to-leg coupling ratio $\tilde{K}$ and (c) energy bias $\tilde{\omega}$, and phase boundary of the AVP with different (b) energy biases $\tilde{\omega}$ and (d) atomic interactions $\tilde{U}$. The other parameter is $\phi = \pi/2$.

IV. DYNAMICAL ASYMMETRIC VORTEX STATE

When considering the time evolution effect caused by the energy difference between two states of the superposition state, a different type of DAVS will occur. For the BEC in an asymmetric double-well potential, a time dependent interference pattern has been observed in the experiment [72]. Recently, the scheme for realizing spin-tensor momentum coupling of spin-1 atoms predicted a possible way to discover such different types of dynamical stripe states [73,74]. Due to the energy difference between middle and bottom bands, the corresponding stripe state shows a dynamical phase, which induces a moving stripe pattern [73]. A similar moving stripe pattern caused by the moving lattice potential has been observed in a recent experiment, which realized the stripe phase with supersolid properties in SOC BECs [35]. From similar arguments, one can expect that the superposition of two states with energy difference will induce such dynamical phases.

As previously discussed in Fig. 1(b), the controlled energy bias of the ladder system will induce an energy difference between two states of the superposition state. When we consider the atomic interaction, the structure of the energy band will become more complex, which means the strength of this energy difference will be modified by the atomic interaction. In the case of the AVP discussed in Sec. III, the energy difference between two states is sufficiently weak, and the energy difference induced dynamic effects can be ignored. However, when the energy difference is strong enough, the energy difference induced dynamic effect should be considered and DAVS will occur. In this case, we should consider a new superposition state

$$\begin{bmatrix} a_{m,L} \\ a_{m,R} \end{bmatrix} = \begin{bmatrix} a_{L+}\cos\theta e^{i(mk_+-\varepsilon_+t)} + a_{L-}\sin\theta e^{-i(mk_-+\varepsilon_-t)} \\ a_{R+}\cos\theta e^{i(mk_+-\varepsilon_+t)} + a_{R-}\sin\theta e^{-i(mk_-+\varepsilon_-t)} \end{bmatrix}, \tag{17}$$

where angle θ is given by the variational analysis (4), which determines the superposition coefficients of two different states. The quasimomentum corresponding to the energy minimum point has two different values $k_\pm$, which also can be obtained by the variational analysis (4); the corresponding energy values of two states are $\varepsilon_\pm$, respectively. From the superposition state (17), density distributions of the ladder

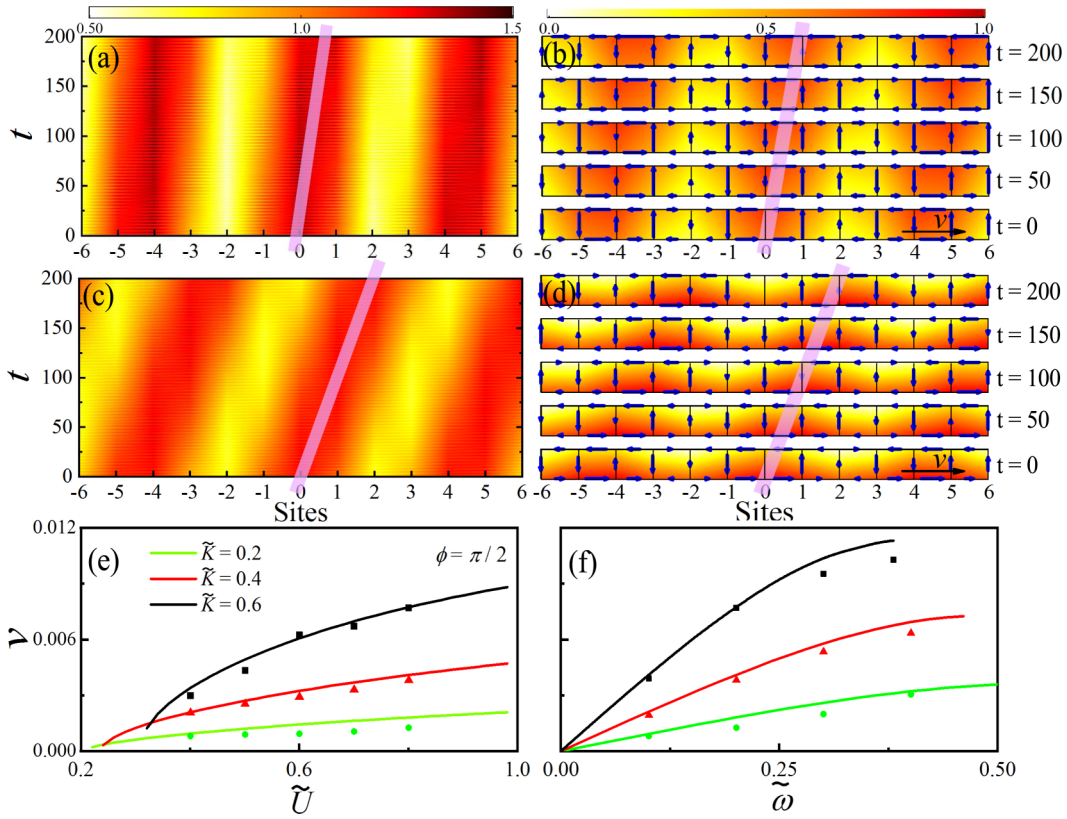

FIG. 6. Time evolution of the sum density obtained by the Runge-Kutta numerical simulation of the GP equation (2) with different energy bias (a) $\tilde{\omega} = 0.1$ and (c) $\tilde{\omega} = 0.4$. (b, d) Corresponding density distributions and local current configurations for variational results at different times $t = 200$, 150, 100, 50, and 0. The colorbar represents the particle density. The other parameters are $\tilde{U} = 0.8$, $\tilde{K} = 0.6$, and $\phi = \pi/2$. (e, f) The velocity of the vortex for different rung-to-leg coupling ratios $\tilde{K}$ vs (e) the atomic interaction and (f) the energy bias. Solid lines correspond to the variational results of Eq. (19), and symbols correspond to numerical simulation results of the GP equation (2).

system are shown to be

$$\begin{aligned} n_{m,L} &= a_{L+}^2 \cos^2\theta + a_{L-}^2 \sin^2\theta \\ &\quad + a_{L+}a_{L-} \sin 2\theta \cos[\Delta\varepsilon t - (k_+ + k_-)m], \\ n_{m,R} &= a_{R+}^2 \cos^2\theta + a_{R-}^2 \sin^2\theta \\ &\quad + a_{R+}a_{R-} \sin 2\theta \cos[\Delta\varepsilon t - (k_+ + k_-)m]. \end{aligned} \tag{18}$$

It is clear that the first two terms mainly determine the asymmetry density distribution of two legs and the last terms result in the periodical density modulations. The energy difference between two states of the superposition state $\Delta\varepsilon = \varepsilon_+ - \varepsilon_-$, which induces the global motion of the vortex structure, i.e., the dynamical phase. The producing mechanism of this dynamical phase is similar to the time dependent interference pattern of two interfered BECs [72]. The motion law of this vortex can be controlled by a velocity $v = \frac{dm}{dt} = \frac{\Delta\varepsilon}{k_+ + k_-}$. This DAVS breaks both translational and Z_2 symmetry of the system, showing dynamical supersolidlike properties. In Figs. 6(a) and 6(c), the time evolutions of the sum density $n_m = n_{m,L} + n_{m,R}$ are plotted by using the Runge-Kutta numerical simulation of the GP equation (2). One immediately sees that the vortex maintains a constant speed through two legs, i.e., a DAVS occurs. Approximately, we assume the energy difference between two states of the superposition state will not change with time. In order to obtain this energy value, we substitute the superposition state (17) into the GP equation (2). For a sufficiently short time dt, the vortex moves only the dm site; the corresponding stationary state Schrödinger equation can be obtained by using the definition of the velocity

$$\begin{aligned} \varepsilon_+ a_{L+} &= -2\cos\left(\frac{\phi}{2} - k_+\right)a_{L+} - \tilde{K}a_{R+} - \frac{\tilde{\omega}}{2}a_{L+} + \tilde{U}\left(a_{L+}^2\cos^2\theta + 2a_{L-}^2\sin^2\theta + \frac{1}{2}a_{L+}a_{L-}\sin 2\theta\right)a_{L+}, \\ \varepsilon_- a_{R-} &= -2\cos\left(\frac{\phi}{2} - k_-\right)a_{R-} - \tilde{K}a_{L-} + \frac{\tilde{\omega}}{2}a_{R-} + \tilde{U}\left(a_{R-}^2\sin^2\theta + 2a_{R+}^2\cos^2\theta + \frac{1}{2}a_{R-}a_{R+}\sin 2\theta\right)a_{R-}, \\ \varepsilon_+ a_{R+} &= -2\cos\left(\frac{\phi}{2} - k_+\right)a_{R+} - \tilde{K}a_{L+} + \frac{\tilde{\omega}}{2}a_{R+} + \tilde{U}\left(a_{R+}^2\cos^2\theta + 2a_{R-}^2\sin^2\theta + \frac{1}{2}a_{R+}a_{R-}\sin 2\theta\right)a_{R+}, \\ \varepsilon_- a_{L-} &= -2\cos\left(\frac{\phi}{2} - k_-\right)a_{L-} - \tilde{K}a_{R-} - \frac{\tilde{\omega}}{2}a_{L-} + \tilde{U}\left(a_{L-}^2\sin^2\theta + 2a_{L+}^2\cos^2\theta + \frac{1}{2}a_{L-}a_{L+}\sin 2\theta\right)a_{L-}. \end{aligned} \tag{19}$$

By solving these sets of equation, we can obtain the value of the energy difference between two states of the superposition state $\Delta\varepsilon$. Substituting $\Delta\varepsilon$ into density distributions (18), we plot the corresponding density distributions and local current configurations at different times $t = 200$, 150, 100, 50, and 0 in Figs. 6(b) and 6(d) for $\tilde{\omega} = 0.1$ and 0.4, respectively, which clearly show the DAVS. As shown by the pink thick lines in Figs. 6(a)–6(d), the vortex moves only one site approximately for $\tilde{\omega} = 0.1$ during $t = 0$–200; with the increase of the energy bias the velocity of the vortex increases, which moves two sites approximately for $\tilde{\omega} = 0.4$. Generally, the velocity of the vortex depends on the atomic interaction, energy bias, rung-to-leg coupling ratio, and magnetic field, which is described in Figs. 6(e) and 6(f). With increasing of the atomic interaction $\tilde{U}$, energy bias $\tilde{\omega}$, and rung-to-leg coupling ratio $\tilde{K}$, the velocity increases, which means that a significant DAVS will appear at the boundary of the phase transition. Different symbols correspond to the numerical simulation results of GP equation (2) with different rung-to-leg coupling ratios, which agree well with the variational results of Eq. (19) (solid lines). It is worth mentioning that the velocity of the vortex is very small in most situations, thus the phase diagrams we have discussed in Sec. III are effective. Moreover, Sec. III demonstrates that the AVP indeed is the ground state with the lowest energy. Therefore, this DAVS also has the low-energy property, which makes the dynamic process of the system more stable and will have more advantages in quantum transport. Meanwhile, due to the breaking of the additional Z_2 symmetry, the imbalance density distribution on two legs of the DAVS provides an additional freedom degree, which means that this state will have greater information carrying ability. Recently, the possibility of realizing a time crystal, the lowest-energy states of which are periodic in time much like ordinary crystals are periodical in space [75,76], has generated extensive attention and heated discussion. Due to the unique periodical vortex structures and low-energy dynamic property of the DAVS, the biased ladder system may be a potential way to study the time crystal by more rigorous design.

V. SUMMARY

In conclusion, by adding the controllable energy bias, we predict full ground-state phase diagrams and depict features of two kinds of plane-wave phase (PWI and PWII) and the AVP in the biased two-leg ladder system. Interestingly, the transition processes can be highly modulated and controlled by the energy bias, atomic interaction, magnetic field, and rung-to-leg coupling ratio. We further studied the excitation spectrum of the plane-wave phase, which provides a different way to distinguish the AVP. Moreover, a different type of DAVS is discussed in detail in this biased ladder system, which may have potential applications for quantum transport and the time crystal. Our paper has instructive significance for exploring novel phases in condensed-matter systems and also opens an intuitive path to investigate relevant phenomena of interacting systems.

ACKNOWLEDGMENTS

This work is supported by the National Natural Science Foundation of China under Grants No. 12164042, No. 11764039, No. 11475027, No. 11865014, and No. 11847304; by the Natural Science Foundation of Gansu province under Grants No. 17JR5RA076 and No. 20JR5RA526; by the Scientific Research Project of Gansu higher education under Grant No. 2016A-005; by the Innovation Capability Enhancement Project of Gansu higher education under Grants No. 2020A-146 and No. 2019A-014; by the Creation of Science and Technology of Northwest Normal University under Grant No. NWNU-LKQN-18-33; and by the Excellent Graduate Innovation Star Project of Education Department of Gansu Province under Grant No. 2021CXZX-180.

[1] J. Bardeen, L. N. Cooper, and J. R. Schrieffer, Phys. Rev. **108**, 1175 (1957).
[2] B. Rosenstein and D. Li, Rev. Mod. Phys. **82**, 109 (2010).
[3] J. Dalibard, F. Gerbier, G. Juzeliūnas, and P. Öhberg, Rev. Mod. Phys. **83**, 1523 (2011).
[4] Y.-J. Lin, R. L. Compton, K. Jiménez-García, J. V. Porto, and I. B. Spielman, Nature (London) **462**, 628 (2009).
[5] N. Goldman, G. Juzeliūnas, P. Öhberg, and I. B. Spielman, Rep. Prog. Phys. **77**, 126401 (2014).
[6] O. Morsch and M. Oberthaler, Rev. Mod. Phys. **78**, 179 (2006).
[7] O. Dutta, M. Gajda, P. Hauke, M. Lewenstein, D.-S. Lühmann, B. A. Malomed, T. Sowiński, and J. Zakrzewski, Rep. Prog. Phys. **78**, 066001 (2015).
[8] H. Sakaguchi and B. A. Malomed, Phys. Rev. E **72**, 046610 (2005).
[9] P. Donohue and T. Giamarchi, Phys. Rev. B **63**, 180508(R) (2001).
[10] E. Orignac and T. Giamarchi, Phys. Rev. B **64**, 144515 (2001).
[11] M. Atala, M. Aidelsburger, M. Lohse, J. T. Barreiro, B. Paredes, and I. Bloch, Nat. Phys. **10**, 588 (2014).
[12] Y.-J. Zhao, X.-W. Xu, H. Wang, Y.-X. Liu, and W.-M. Liu, Phys. Rev. A **102**, 053722 (2020).
[13] Y.-J. Zhao, N. Tan, D. Yu, B. Liu, and W.-M. Liu, Phys. Rev. Research **2**, 033484 (2020).
[14] A. Petrescu and K. Le Hur, Phys. Rev. Lett. **111**, 150601 (2013).
[15] A. Dhar, M. Maji, T. Mishra, R. V. Pai, S. Mukerjee, and A. Paramekanti, Phys. Rev. A **85**, 041602(R) (2012).
[16] M. Di Dio, S. De Palo, E. Orignac, R. Citro, and M.-L. Chiofalo, Phys. Rev. B **92**, 060506(R) (2015).
[17] S. Barbarino, G. Sangiovanni, and J. C. Budich, Phys. Rev. B **99**, 075158 (2019).
[18] T. Sun, Y. Zheng, S.-J. Yang, and S. Yang, Phys. Rev. A **103**, 013316 (2021).
[19] G. Sun, Phys. Rev. A **93**, 023608 (2016).
[20] Y. Zheng, S. Feng, and S.-J. Yang, Phys. Rev. A **96**, 063613 (2017).
[21] J. Zurita, C. E. Creffield, and G. Platero, Adv. Quantum Technol. **3**, 1900105 (2020).
[22] S. Sajid and A. Chakrabarti, Phys. Rev. B **102**, 134401 (2020).
[23] D. Hügel and B. Paredes, Phys. Rev. A **89**, 023619 (2014).
[24] X. Yin, T.-L. Ho, and X. Cui, New J. Phys. **21**, 013004 (2019).

[25] H. Deng, H. Dai, J. Huang, X. Qin, J. Xu, H. Zhong, C. He, and C. Lee, Phys. Rev. A **92**, 023618 (2015).
[26] W. Tschischik, M. Haque, and R. Moessner, Phys. Rev. A **86**, 063633 (2012).
[27] Y. Zheng, S. Feng, and S.-J. Yang, Phys. Rev. A **97**, 043627 (2018).
[28] W. Tschischik, R. Moessner, and M. Haque, Phys. Rev. A **92**, 023845 (2015).
[29] R. Jafari, H. Johannesson, A. Langari, and M. A. Martin-Delgado, Phys. Rev. B **99**, 054302 (2019).
[30] M. E. Tai, A. Lukin, M. Rispoli, R. Schittko, T. Menke, D. Borgnia, P. M. Preiss, F. Grusdt, A. M. Kaufman, and M. Greiner, Nature (London) **546**, 519 (2017).
[31] F. A. An, E. J. Meier, and B. Gadway, Sci. Adv. **3**, e1602685 (2017).
[32] L. F. Livi, G. Cappellini, M. Diem, L. Franchi, C. Clivati, M. Frittelli, F. Levi, D. Calonico, J. Catani, M. Inguscio, and L. Fallani, Phys. Rev. Lett. **117**, 220401 (2016).
[33] B. Stuhl, H.-I. Lu, L. Aycock, D. Genkina, and I. Spielman, Science **349**, 1514 (2015).
[34] M. Mancini, G. Pagano, G. Cappellini, L. Livi, M. Rider, J. Catani, C. Sias, P. Zoller, M. Inguscio, M. Dalmonte *et al.*, Science **349**, 1510 (2015).
[35] J.-R. Li, J. Lee, W. Huang, S. Burchesky, B. Shteynas, F. Ç. Top, A. O. Jamison, and W. Ketterle, Nature (London) **543**, 91 (2017).
[36] J.-Y. Zhang, S.-C. Ji, Z. Chen, L. Zhang, Z.-D. Du, B. Yan, G.-S. Pan, B. Zhao, Y.-J. Deng, H. Zhai, S. Chen, and J. W. Pan, Phys. Rev. Lett. **109**, 115301 (2012).
[37] X. Y. Yin, S. Gopalakrishnan, and D. Blume, Phys. Rev. A **89**, 033606 (2014).
[38] M. Piraud, F. Heidrich-Meisner, I. P. McCulloch, S. Greschner, T. Vekua, and U. Schollwoeck, Phys. Rev. B **91**, 140406(R) (2015).
[39] E. Orignac, R. Citro, M. Di Dio, S. De Palo, and M.-L. Chiofalo, New J. Phys. **18**, 055017 (2016).
[40] A. Keleş and M. O. Oktel, Phys. Rev. A **91**, 013629 (2015).
[41] C. Romen and A. M. Läuchli, Phys. Rev. B **98**, 054519 (2018).
[42] A. Dhar, T. Mishra, M. Maji, R. V. Pai, S. Mukerjee, and A. Paramekanti, Phys. Rev. B **87**, 174501 (2013).
[43] S. Greschner, M. Piraud, F. Heidrich-Meisner, I. P. McCulloch, U. Schollwöck, and T. Vekua, Phys. Rev. Lett. **115**, 190402 (2015).
[44] S. Greschner, M. Piraud, F. Heidrich-Meisner, I. P. McCulloch, U. Schollwöck, and T. Vekua, Phys. Rev. A **94**, 063628 (2016).
[45] S. Greschner and T. Vekua, Phys. Rev. Lett. **119**, 073401 (2017).
[46] M. Calvanese Strinati, R. Berkovits, and E. Shimshoni, Phys. Rev. B **100**, 245149 (2019).
[47] F. Crépin, N. Laflorencie, G. Roux, and P. Simon, Phys. Rev. B **84**, 054517 (2011).
[48] A. Petrescu, M. Piraud, G. Roux, I. P. McCulloch, and K. Le Hur, Phys. Rev. B **96**, 014524 (2017).
[49] A. Petrescu and K. Le Hur, Phys. Rev. B **91**, 054520 (2015).
[50] S. Greschner, M. Filippone, and T. Giamarchi, Phys. Rev. Lett. **122**, 083402 (2019).
[51] M. Filippone, C.-E. Bardyn, S. Greschner, and T. Giamarchi, Phys. Rev. Lett. **123**, 086803 (2019).
[52] E. Cornfeld and E. Sela, Phys. Rev. B **92**, 115446 (2015).
[53] M. Calvanese Strinati, E. Cornfeld, D. Rossini, S. Barbarino, M. Dalmonte, R. Fazio, E. Sela, and L. Mazza, Phys. Rev. X **7**, 021033 (2017).
[54] M. Buser, F. Heidrich-Meisner, and U. Schollwöck, Phys. Rev. A **99**, 053601 (2019).
[55] B. Wang, X.-Y. Dong, F. N. Ünal, and A. Eckardt, New J. Phys. **23**, 063017 (2021).
[56] R. Wei and E. J. Mueller, Phys. Rev. A **89**, 063617 (2014).
[57] M. Buser, C. Hubig, U. Schollwöck, L. Tarruell, and F. Heidrich-Meisner, Phys. Rev. A **102**, 053314 (2020).
[58] G. I. Martone, Euro. Phys. J. Spec. Top. **224**, 553 (2015).
[59] W. Zheng, Z.-Q. Yu, X. Cui, and H. Zhai, J. Phys. B **46**, 134007 (2013).
[60] C. Chin, R. Grimm, P. Julienne, and E. Tiesinga, Rev. Mod. Phys. **82**, 1225 (2010).
[61] A. R. Kolovsky, Europhys. Lett. **93**, 20003 (2011).
[62] C. J. Kennedy, G. A. Siviloglou, H. Miyake, W. C. Burton, and W. Ketterle, Phys. Rev. Lett. **111**, 225301 (2013).
[63] G. Roux, E. Orignac, S. R. White, and D. Poilblanc, Phys. Rev. B **76**, 195105 (2007).
[64] A. Tokuno and A. Georges, New J. Phys. **16**, 073005 (2014).
[65] Y. Li, L. P. Pitaevskii, and S. Stringari, Phys. Rev. lett. **108**, 225301 (2012).
[66] Z. Chen and Z. Liang, Phys. Rev. A **93**, 013601 (2016).
[67] W. Han, G. Juzeliūnas, W. Zhang, and W.-M. Liu, Phys. Rev. A **91**, 013607 (2015).
[68] M. A. Khamehchi, Y. Zhang, C. Hamner, T. Busch, and P. Engels, Phys. Rev. A **90**, 063624 (2014).
[69] S.-C. Ji, L. Zhang, X.-T. Xu, Z. Wu, Y. Deng, S. Chen, and J.-W. Pan, Phys. Rev. Lett. **114**, 105301 (2015).
[70] X. Xu, Z. Zhang, and Z. Liang, Phys. Rev. A **100**, 053616 (2019).
[71] Z.-Q. Yu, Phys. Rev. A **93**, 033648 (2016).
[72] Y. Shin, M. Saba, T. A. Pasquini, W. Ketterle, D. E. Pritchard, and A. E. Leanhardt, Phys. Rev. Lett. **92**, 050405 (2004).
[73] X.-W. Luo, K. Sun, and C. Zhang, Phys. Rev. Lett. **119**, 193001 (2017).
[74] J. Sun, Y. Chen, X. Chen, and Y. Zhang, Phys. Rev. A **101**, 053621 (2020).
[75] K. Sacha and J. Zakrzewski, Rep. Prog. Phys. **81**, 016401 (2017).
[76] J. Zakrzewski, Physics **5**, 116 (2012).